Syntheses of novel 1,5-Benzodiazepine derivatives: crystal structures, spectroscopic characterizations, Hirshfeld surface analyses, molecular docking studies, DFT calculations, corrosion inhibition anticipation and antibacterial activities

Lhoussaine El Ghayati[a], Yusuf Sert[b], Nada Kheira Sebbar[a,c*], Youssef Ramli[d], Noureddine Hamou Ahabchane[a], Ahmed Talbaoui [e], Joel T. Mague[f] , Brahim El Ibrahimi[g], Mohamed Labd Taha[c], El Mokhtar Essassi[a], Nabil Al-Zaqri[h*], Ali Alsalme[h].

[a]Laboratory of Heterocyclic Organic Chemistry, Medicines Science Research Center, Pharmacochemistry Competence Center, Mohammed V University in Rabat, Faculté des Sciences, Av. Ibn Battouta, BP 1014 Rabat, Morocco. [b]Bozok University Department of Physics Yozgat/Turkey; [c]Laboratory of Chemistry and Environment, Applied Bioorganic Chemistry Team, Faculty of Sciences, Ibn Zohr University, Agadir, Morocco; [d]Laboratory of Medicinal Chemistry, Drug Sciences Research Center, Faculty of Medicine and Pharmacy, Mohammed V University, Rabat, Morocco; [e]Laboratoire de Biologie des Pathologies Humaines, Faculté des Sciences, Université Mohammed V, Rabat, Morocco; [f]Department of Chemistry, Tulane University, New Orleans, LA 70118, USA; [g]Applied Chemistry-Physic Team, Faculty of Sciences, University of Ibn Zohr, Agadir, Morocco. [h]Department of chemistry, College of Science, King Saud University, P.O. Box 2455, Riyadh 11451, Saudi Arabia.

_____

Corresponding authors: [h]Department of chemistry, College of Science, King Saud University, P.O. Box 2455, Riyadh 11451, Saudi Arabia; E-mail: nalzaqri@ksu.edu.sa (N. Al-Zaqri).
[c]*Laboratory of Chemistry and Environment, Applied Bioorganic Chemistry Team, Faculty of Sciences, Ibn Zohr University, Agadir, Morocco;* E-mail: snounousebbar@gmail.com (N.K.SEBBAR).

Abstract

A series of newly pyrazolo-1,5-benzodiazepine derivatives (**5-7**) was performed and characterized by using ^{1}H, ^{13}C-NMR spectroscopic measurements. The molecular and crystal structures of two compounds **2** and **7** have also been further examined by single-crystal X-ray crystallography showing that the alkyl groups are beard by sulfur atom and to pyrazolic nitrogen atom in position 2 and not in position 1 of the tricyclic compounds as described in the literature. In addition, through Hirshfeld surface analysis, molecular docking studies and DFT calculations, the closest contact between the active atoms of the compound can be determined. Also, the Monte Carlo simulations outcomes show that compounds **2** and **7** can be considered as a good acidic corrosion inhibitor for the aluminum metal, while emphasizing that the compound **7** provides enhanced prevention. Finally, compounds **1** to **7** were evaluated for their antibacterial activity against Gram-positive and Gram-negative microbial strains such as *Escherichia coli*, *Pseudomonas aeruginosa*, *Staphylococcus aureus* and *Streptococcus*. The results obtained demonstrated the

This article has been accepted for publication and undergone full peer review but has not been through the copyediting, typesetting, pagination and proofreading process which may lead to differences between this version and the Version of Record. Please cite this article as doi: 10.1002/jhet.4167

antibacterial activity of compounds 1 to 7 tested using the minimal inhibitory concentration (MIC).

Keywords: 1,5-benzodiazepines, Hirshfeld surface, Crystal, Molecular docking, DFT, Monte Carlo simulation, Antibacterial activity.

I | INTRODUCTION

The field of heterocyclic chemistry has become increasingly important in recent years. Indeed, the heterocyclic structures, whether of synthetic or natural origin, appear as a particularly interesting support in very varied areas (pharmacy, medicine, industry .....) [1-4]. It is noted that two-thirds of the organic compounds, known in the literature, are heterocycles: containing at least one heteroatom (most often nitrogen, oxygen or sulfur) [8-11]. In particular, 1,5-benzodiazepines are well-known for their various therapeutic properties including anticonvulsant, anti-inflammatory, analgesic, hypnotic, sedative and hypnotic activities [12-17]. They are also used to relieve pain of skeletal muscle joints and the spasticity resulting from cerebral palsy and paraplegia, athetosis and stiff-man syndrome. Recently they have been reported to show antileukamic, antiplatelet, antilucer, endothelia antagonist and vasopressin antagonist activities [18]. In addition, benzodiazepines are a useful precursor for the synthesis of other fused ring compounds such as triazolo-, oxadiazolo, oxazino-, furano or pyrazolo-benzodiazepines [19-23]. Benzodiazepines (BZD) are classified as drugs known for their remarkable activity on the central nervous system (CNS) [24]. The area of biological interest of 1,5-benzodiazepines [25] is extended to various diseases such as cancer [26], viral infection (non-nucleoside reverse transcriptase inhibitors of HIV-1 [27-29] and cardiovascular disorders [27-30]. Indeed, the nucleus 1,5-benzodiazepine is a preferred carrier existing in active compounds belonging to a variety of biological targets such as peptide hormones (Cholecystokinins CCKA and CCKB) [31-33], enzymes interleukins ICE [34-36] and potassium inhibitors (Ik) [30] (Scheme 1).

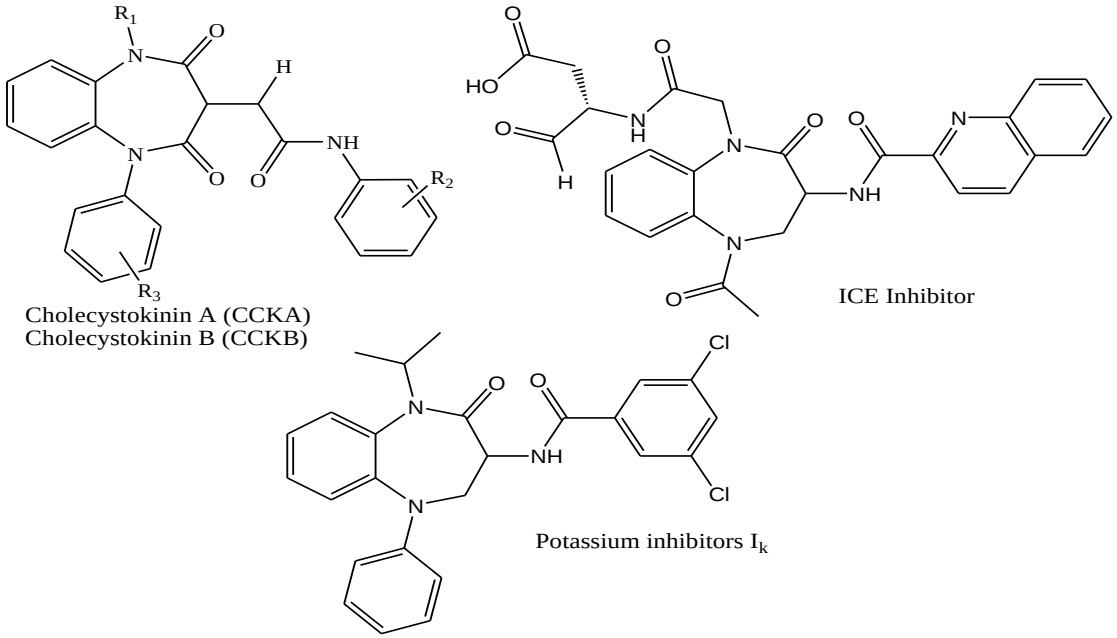

Scheme 1. Examples of bioactive molecules derived from 1,5-benzodiazepine.

In continuation of our previous works [23, 37-39], we are interested in the preparation of condensed nitrogen heterocyclic compounds containing 1,5-benzodiazepine nucleus (**5-7**). Their structures were clarified on the basis of spectral data and confirmed by single-crystal X-ray diffraction in the case of compounds **2** and **7**. They are also characterized using DFT to compute and predict the corresponding spectral data and Z matrix coordinates at the B3LYP / 6-31G (d, p) level and at the theoretical level. The molecular docking studies from the Protein Data Bank (4GQS) on an inhibitor were carried out using Auto-Dock Vina program. Moreover, aluminum, copper and iron metals, as well as their alloys, are widely used in various industrial applications due to their attractive physicochemical properties. Nonetheless, the contact of these metallic materials with aggressive environments (i.e. acid media) throughout their utilization involves their degradation, which leads to noticeable economic and safety loss [40]. As a solution to overcome this problematic, the use of corrosion inhibitors, such as organic-based compounds, is required [41]. Recently, the Monte Carlo simulations have been used to investigate the adsorption process of several organic inhibitors onto different metallic surfaces [42]. Conferring to the obtained computational data, the adsorption energy (or binding energy) was effectively correlated with the observed inhibition effectiveness. From which, the higher protection ability of an organic inhibitor has been associated with its great adsorption energy on the metal surface [43-44]. In this context, we further aim in this work to expect the tendency of the newly synthesized compounds to prevent the corrosion of aluminum, copper and iron in acidic medium using this theoretical approach. Finally, compounds (1-7) were evaluated for their antibacterial

activity against Gram-positive and Gram-negative bacteria such as *Escherichia coli, Pseudomonas aeruginosa, Staphylococcus aureus and Streptococcus.*

2 | RESULTS AND DISCUSSION

2.1. Chemical synthesis of 1,5-benzodiazepines 5-7

Initially, we prepared 1-ethyl-4-phenyl-1,5-benzodiazpine-2-thione **2** by sulfurization of 1-ethyl-4-phenyl-1,5-benzodiazpin-2-one **1** [45] with phosphorus pentasulfide (P_2S_5) added in small portions to the freshly distilled pyridine. The reaction mixture was heated to 100°C for 4 hours (**Step a**). Thereafter, 3-[N-2-(aminophenyl)-N-ethylamino]-5-phenylpyrazole **3** was obtained by condensation of hydrazine hydrate with compound **2** (**Step b**) (Scheme 2). It is worthy to note that in a previous work [23] concerning the action of 3-[*N*-2-(aminophenyl)-*N*-ethylamino]-5-phenylpyrazole **3** with carbon disulfide in refluxing pyridine, we isolated in all cases a single product whose structure could correspond to pyrazolo-1,3,5-benzotriazepine-4-thione **4A** or to pyrazolo 1,5-benzodiazepine-4-thione **4B** (**Step c**) (Scheme 2). To differenciate between the two structures A and B, we have used a chemical method consisting of the alkylation of the compound obtained under solid-liquid phase transfer catalysis conditions by various alkylating agents (methyl iodide, ethyl and allyl bromide). In all cases we isolated a single dialkylated compound, allowing to reject the structure **4A** which would lead, under the same reaction conditions, to a monoalkylated compound coming from the alkylation of the sulfur atom of the thioamide group of the seven membered rings. As an extension of this work and in order to reexamine the structures of compounds obtained, we proceeded to the alkylation of compound **4B** by other alkylating agents: such as propargyl bromide, benzyl chloride and ethyl bromoacetate in DMF in the presence of K_2CO_3 as base, and tetra n-butyl ammonium bromide (TBAB) as catalyst. In all cases we have isolated the dialkylated pyrazolobenzodiazepine **5-7** in good yields (**Step d**); (Scheme 2).

To confirm the structure of compounds **5-7** a crystallography study of compound **7** has been undertaken showing that the two ethoxycarbonyl methyl groups are beared by the sulfur atom and the pyrazolic nitrogen atom in position 2 and not in position 1 of the tricyclic compound **7** as proposed by the authors [23].

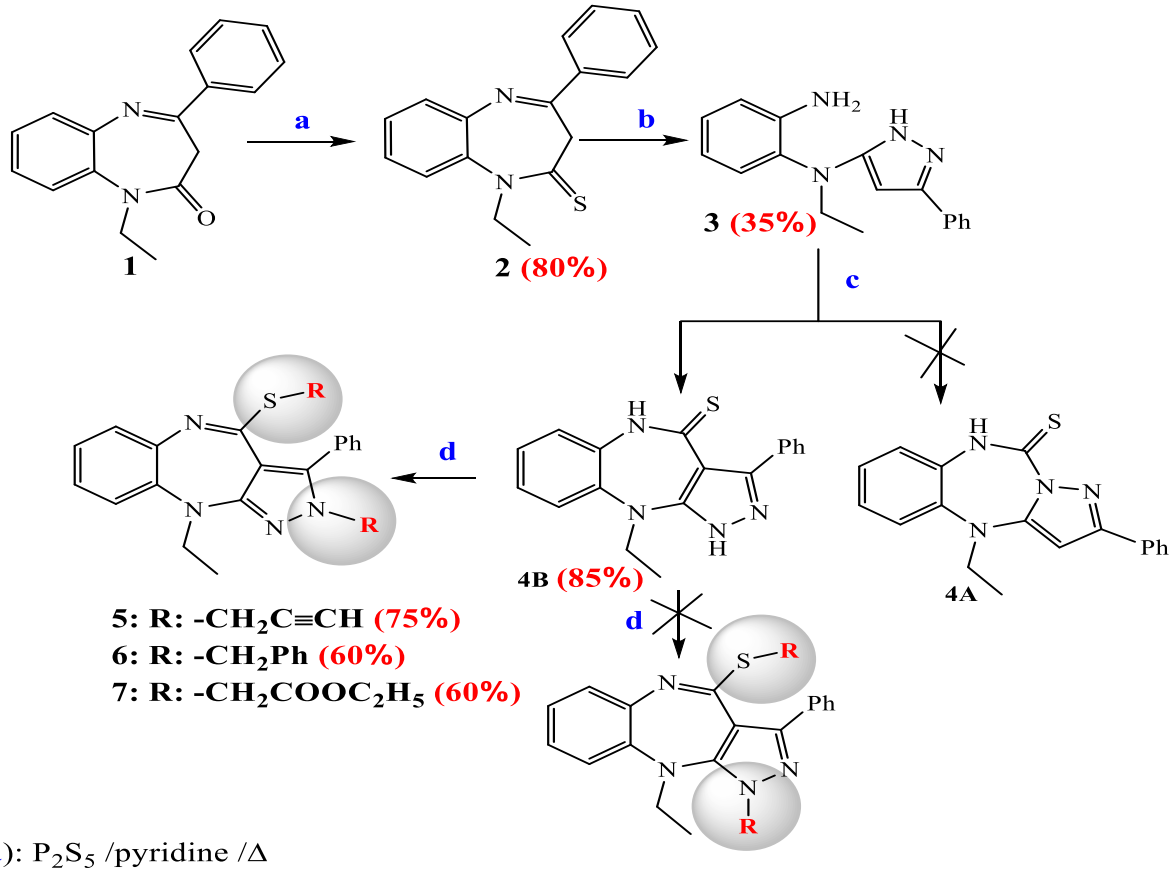

(**a**): P_2S_5 /pyridine /Δ
(**b**): NH_2NH_2 /CH_3CH_2OH/rt, 48 h
(**c**): CS_2 /pyridine /rt, 24 h
(**d**): X-**R:** Br**$CH_2C{\equiv}CH$**, Cl**CH_2Ph**, Br**$CH_2COOC_2H_5$**, DMF, K_2CO_3, TBAB, rt, 24 h

Scheme 2. Synthesis of 1,5-benzodiazépine-2-thione derivatives: **2-7**.

A plausible mechanism has been proposed for the formation of compound **3** (**Scheme 3)**: the initial step corresponds to the attack of the amino group of hydrazine on the carbon atom of the thiocarbonyl group of the seven membered ring leading to the intermediate [A] which undergoes to an intramolecular cyclization involving the hydrazine amino group and the electrophilic carbon atom of the in position 4 of the bicyclic compound to afford the instable tricyclic compound [B]. The latter, after the cleavage of C_4-N_5 bond leads to the pyrazolic compound [C] which after the loss of a hydrogen sulfide molecule gives the compound **3**.

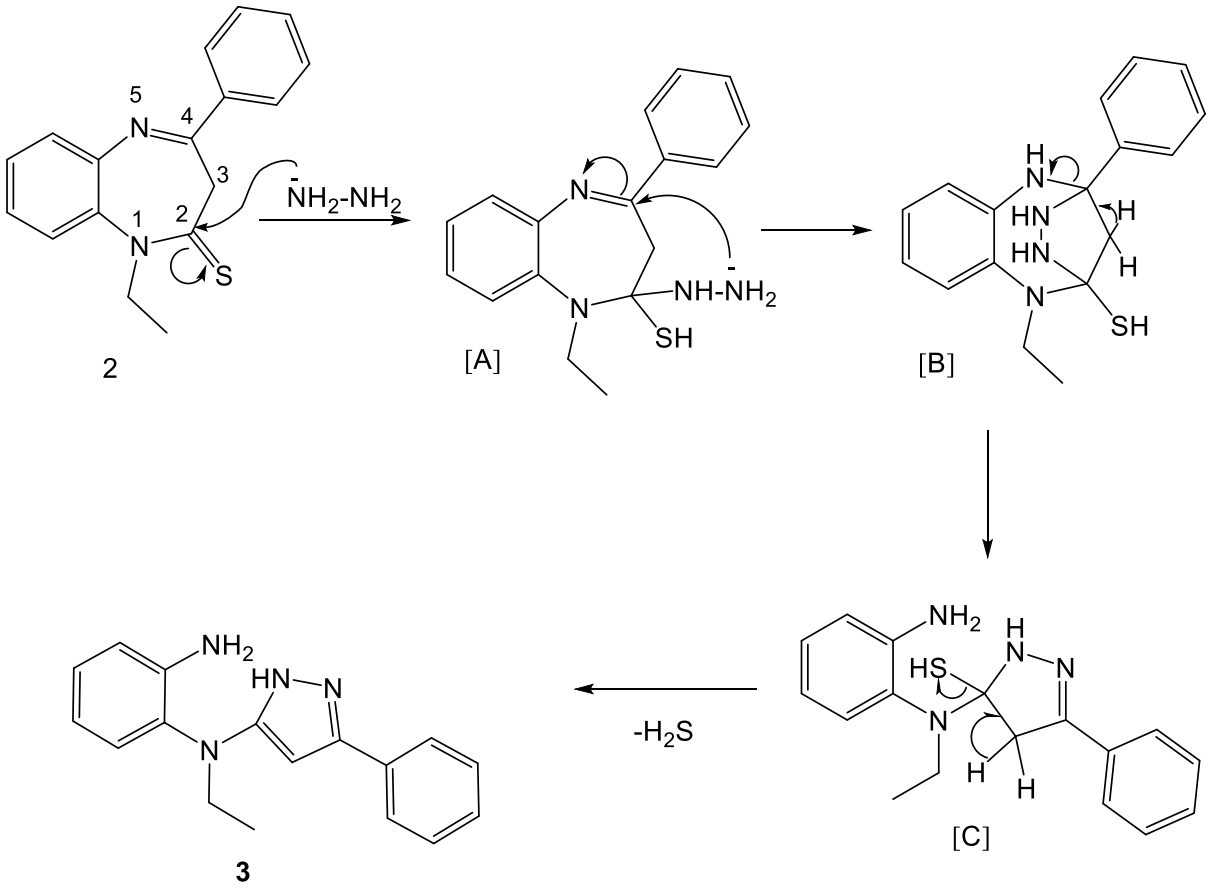

Scheme 3. Plausible mechanism for synthesis of compound **3**

Also, a plausible mechanism proposed for the formation of compound **4B** is depicted in scheme 4: the amino group of compound **3** attacks the carbon atom of carbon disulfide to lead after a loss of a hydrogen sulfide molecule to the isothiocyanate intermediate [D]. which undergoes an intramolecular cyclization corresponding to the attack of the nucleophilic pyrazolic carbon atom on the isothiocyanate carbon atom leading to the tricyclic compound [D]. which aromatizes to compound [E] that may exist under the tautomeric form **4B**.

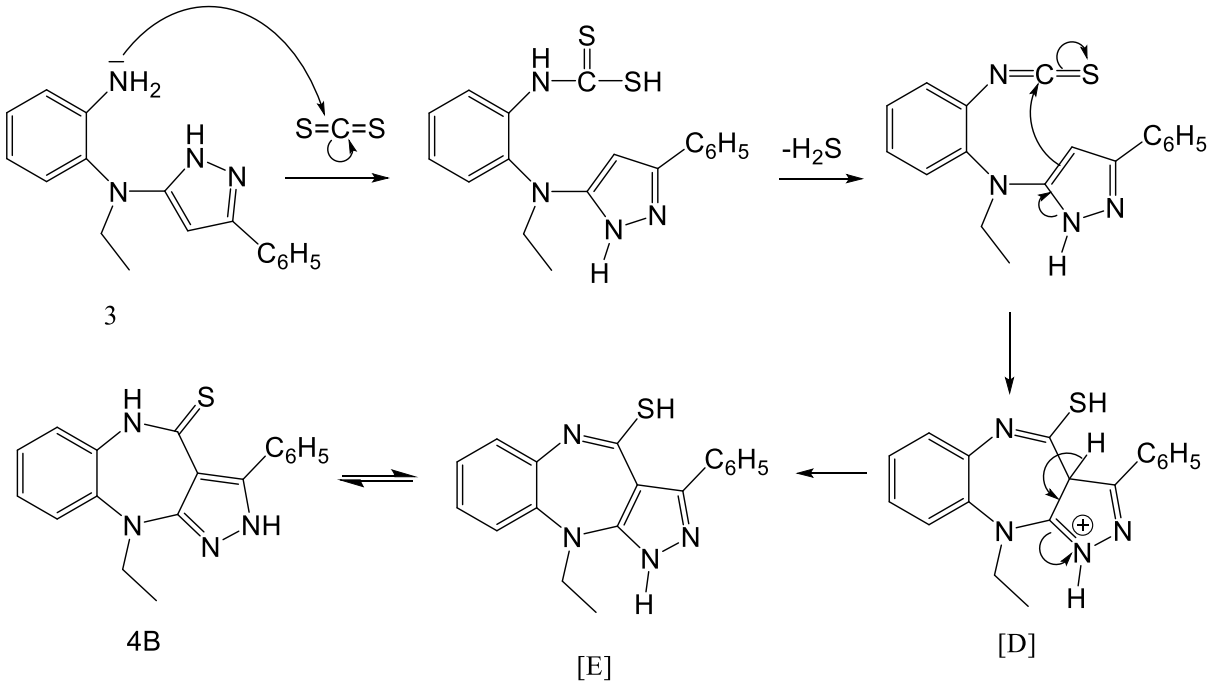

Scheme 4. Plausible mechanism for synthesis of compound **4B**

2.2. Crystal structures of 1,5-benzodiazepine derivatives: 2 and 7.

The title compounds 1,5-benzodiazepine derivatives (**2** and **7**) was selected and X-ray intensity data were collected at 100 K on a Bruker D8 VENTURE PHOTON 100 CMOS diffractometer equipped with an X-ray generator operating at 50 kV and 10 mA, using CuKα radiation. A complete data set was processed using SAINT. The 3D structure (Figure 1) was solved by direct methods (SHELXT) and refined by full matrix, least-squares methods on F2 using SHELXL. The crystallographic analysis of the 1,5-benzodiazepine derivatives (**2** and **7**) obtained by cyclic condensation, N-3 deprotection and alkylation reactions confirmed that the structure of the compound is shown in Figure 1 and Table 1. Interestingly, these compounds crystallize in orthorhombic (**2**) and monoclinic (**7**) crystals, and this system has space groups of $P2_12_12_1$ (**2**) and $P121/n_1$ (**7**). The crystallographic data have been assigned to the CCDC deposit number (see Table 1).

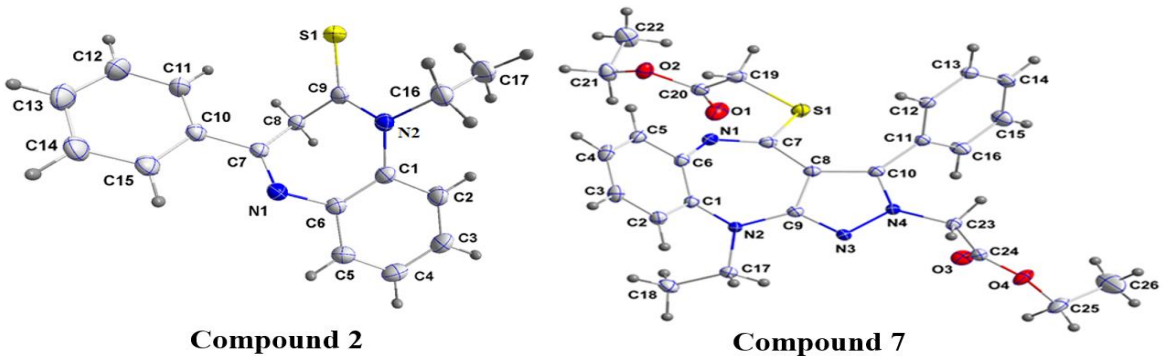

Figure 1: ORTEP d plots, where the ellipsoids are drawn at the 50% probability level of the compounds (**2** and **7**).

Table 1. Experimental Details

	Compound **2**	Compound **7**
Crystal data		
Chemical formula	$C_{17}H_{16}N_2S$	$C_{26}H_{28}N_4O_4S$
CCDC Deposition number	1523021	1958927
Mr	*280.38*	*492.58*
Crystal system, space group	*Orthorhombic, $P2_12_12_1$*	*Monoclinic, P 121/n 1*
Temperature (K)	*296*	*120(2)*
a, b, c (Å)	*8.4001 (8), 9.6239 (9), 18.0037 (18)*	*12.1229(12), 8.8222(8), 23.626(2)*
β (°)	-	*101.407 (2)*
V (Å3)	*1455.5 (2)*	*2476.9(4)*
Z	*4*	*4*
Radiation type	*Mo K_α*	*Mo-Kα*
μ (mm−1)	*0.21*	*0.171*
Crystal size (mm)	*0.32× 0.14 × 0.05*	*0.207 x 0.218 x 0.314*
Diffractometer	*Bruker SMART APEX CCD*	*Bruker Smart APEX CCD*
No. of measured, independent and observed [I> 2σ(I)] reflections	*13778, 3544, 2226*	*46470, 6622, 5595*
Rint	*0.050*	*0.033*
R[F2> 2σ(F2)], wR(F2), S	*0.045, 0.117, 1.02*	*0.038, 0.110, 1.07*
No. of reflections	*3544*	*6622*
No. of parameters	*183*	*417*
Δρmax, Δρmin (e Å−3)	*0.30, -0.14*	*0.48, −0.21*

2.3. *Theoretical details and Hirshfeld details*

The basic idea that DFT is based on is that the energy of the molecule can be determined using electron density instead of wave function. The superiority of DFT methods is that electron correlations are included in the calculations and the obtained results are in better agreement with the experimental results. It also requires less calculation and DFT is a variational method. From here in this work, the three-dimensional geometries of the compound **2** and **7** were drawn in the GaussView interface package program [46] and calculated in the gas phase in the GAUSSIAN 09 package program [47]. The theoretical calculations were performed using the Density Functional Theory (DFT)/Becke-3-LeeYang-Parr (B3LYP) [48-50]. which is a quantum mechanical method. In the Hirshfeld surface analysis section aimed at studying molecular interactions and possible hydrogen bonds, calculations were performed using the Crystal Explorer 3.1 program [51]. Subsequently, after optimization in chloroformic solution, the highest occupied molecular orbital (HOMO) and the lowest unoccupied molecular orbital (LUMO) of compounds **2** and **7** were analyzed. Then, use the functional atomic orbital method B3LYP and 6-31G (d, p) basis, GIAO-Gauge-Inclusive to calculate the theoretical ^{1}H and ^{13}C NMR chemical displacements of compounds **2** and **7**, and compare them with the experimental NMR

spectra in a chloroform solvent. In this manuscript, the ligands of compounds **2** and **7** and the PDB: 4GQS code were generated using the Auto Dock Vina software [52].

2.3.1. *Molecular Geometric Structure*

In this section, use the B3LYP function and the 6-31G (d, p) base level to calculate the optimal structures (bond length and angle) of compounds **2** and **7** in the crystallographic information file (cif). The optimized structure is shown in Figure 2 [46-50]. Additionally, the obtained some selected experimental and theoretical values were listed in Table 2. As seen from the Table 2, there is some inconsistencies between experimental and theoretical results, this is due to phase differences. Because the obtained experimental results are taken in solid phase, while theoretical results are taken in gas phase (ideal situation). To our best knowledges according to literature, no computational and experimental analyses on compound **2** and **7** were reported or published.

Now, let's look at some results (bond lenghts and angles) for both compound **2** and **7**, respectively. In this study for compound **2**, N1-C7, N1-C6, N3-C9 and N3-C1 bond lenghts were computed at 1.289, 1.391, 1.363 and 1.432 Å and observed at 1.274, 1.409, 1.353 and 1.434 Å in x-ray, respectively. The same group looking at Compound **7**; N1-C7, N1-C6, N2-C9 and N2-C1 bond lenghts were calculated at 1.282, 1.405, 1.396 and 1.430 Å with B3LYP function and 6-31G(d,p) basis set. Also, these distances in experimental x-ray study were observed as 1.2827, 1.4206, 1.3930 and 1.4319 Å, respectively. In the literature, 7-chloro-2-methylamino-5-phenyl-3H-1,4-benzodiazepine-4-oxide [51], N1-C2, N1-C7, N4-C3 and N4-C5 (depending on their numbering format) are calculated as 1, 269 / 1.293, 1.391 / 1.390, 1.464 / 1.487 and 1.284 / 1.333Å using HF / B3LYP and base 6-31G (d, p) respectively. According to the reports, based on experiments, these binding times are 1.260, 1.260, 1.500 and 1.300 Â [51]. In our study of compound **2**, with B3LYP function and base pairs 6-31G (d, p), the calculated C9-S1 (thione) bond length is 1.672 Å, while that observed in B2LYP is 1.667 Å [51] X-ray data. On the other hand, for compound 7, the calculated values of the SI-C7 and SI-C19 bond lengths (sulfanyl groups) are 1.791 and 1.817 Â, respectively, and are reported as 1.7729 and 1.7948 Â, respectively as experimental. For 2 - [[(2-methoxy) sulfanyl] -4-(2-methylpropyl)-6-oxo-1,6-dihydropyrimidine-5-carbonitrile [53] S1-C10 (depending on its numbering format), the bond length calculated with the function B3LYP / M06-2X and base 6-31G (d, p) is 1.837 / 1.820 Å, which is reported as 1.800 Å based on experiments.

Next, let's look at some of the binding angles of the results for compounds 2 and 7, respectively. In compound 2, the bond angles C9-N3-C1, C7-N1-C6, N1-C7-C8, N3-C9-C8, N3-C9-S1 and C8-C9-S1 are calculated as 123.5, 121.5, 120.4, 114.5, 124.8 and 120, 6 ° Å have the function B3LYP, and the base 6-31G (d, p) is fixed, and these angles are reported as 122.8, 120.0, 120.8, 115.5, 124.2 and 120.2 ° respectively by experiments. In compound 7, the bond angles C7-S1-C19, C7-N1-C6, C9-N2-C1, N1-C7-C8 and N1-C7-S1 are calculated as 99.8, 125.5, fixed B3LYP function and 6-31G (d, p) base angles of 115.7, 126.5 and 117.8°, which were reported as 101.14, 123.53, 114.67, 126, 62 and 119.42°, respectively in the experiments. For the molecule 7-chloro-2-methylamino-5-phenyl-3H-1,4-benzodiazepine-4-oxide molecule [51], C2-N1-C7, N1-C2-C3, N1-C7-C6, C3-N4-C5, N4-C5-C6 and C5-C6-C7 bond angles (depending on their numbering format) were calculated at 120.2/119.9, 122.2/122.2, 125.2/125.2, 120.0/118.7, 120.0/119.7 and 123.3/124.2° respectively with HF/B3LYP functionals and base 6-31G(d,p). These bond angles were reported experimentally as 115.0, 115.1, 120.0, 106.8183, 120.0 and 120.0°, respectively [51]. In addition, comparison of the selected theoretical results with the B3LYP function and the 6-31G base set (d, p) shows excellent agreement, and further results of optimized molecular structure can be studied using the following method Table 2.

Table 2. Selection of optimized structure parameters of the compounds **2** and **7**.

Bond angles (°)			Bond lenghts (Å)		
Optimized bond angles	X-Ray	DFT/B3LYP/ 6-31 G(d,p)	Optimized bond lenghts	X-Ray	DFT/B3LYP/ 6-31 G(d,p)
Compound **2**					
C9-N2-C16	119.3(2)	119.1	S1-C9	1.657(3)	1.672
C9-N2-C1	122.8(2)	123.5	N1-C7	1.274(3)	1.289
C7-N1-C6	120.0(2)	121.5	N1-C6	1.409(4)	1.391
C1-N2-C16	117.9(2)	117.4	N2-C9	1.353(4)	1.363
C2-C1-C6	118.3(3)	118.7	N2-C1	1.434(4)	1.432
C2-C1-N2	118.4(3)	118.2	N2-C16	1.476(4)	1.486
C6-C1-N2	123.3(2)	123.0	C1-C2	1.391(4)	1.407
C5-C6-N1	116.4(3)	115.7	C1-C6	1.405(4)	1.423
C1-C6-N1	125.0(2)	125.9	C2-C3	1.367(4)	1.388
N1-C7-C10	118.7(2)	118.9	C2-H2	0.9300	1.083
N1-C7-C8	120.8(2)	120.4	C3-C4	1.383(5)	1.399
N3-C9-C8	115.5(2)	114.5	C3-H3	0.930	1.085
N3-C9-S1	124.2(2)	124.8	C4-C5	1.368(5)	1.385
C8-C9-S1	120.2(2)	120.6	C4-H4	0.9300	1.086
C11-C10-C15	119.1(3)	118.8	C5-C6	1.386(4)	1.411
C11-C10-C7	121.7(3)	121.9	C5-H5	0.9300	1.085
C15-C10-C7	119.2(3)	119.3	C7-C10	1.493(4)	1.481
Compound **7**					
C7-S1-C19	101.14(5)	99.8	S1-C7	1.7729(11)	1.791
C20-O2-C21	116.77(9)	116.2	S1-C19	1.7948(11)	1.817
C24-O4-C25	117.05(9)	116.7	O1-C20	1.1994(14)	1.209
C7-N1-C6	123.53(9)	125.5	O2-C20	1.3416(14)	1.352
C9-N2-C1	114.67(8)	115.7	O2-C21	1.4574(14)	1.448
C9-N2-C17	116.52(8)	116.8	O3-C24	1.2026(13)	1.210
C1-N2-C17	119.48(8)	119.8	O4-C24	1.3356(13)	1.345

C9-N3-N4	103.67(8)	104.5	O4-C25	1.4668(14)	1.453
C10-N4-N3	113.16(8)	113.1	N1-C7	1.2827(14)	1.282
C10-N4-C23	128.66(9)	129.6	N1-C6	1.4206(14)	1.405
N3-N4-C23	117.88(8)	117.2	N2-C9	1.3930(13)	1.396
C2-C1-C6	119.46(10)	118.7	N2-C1	1.4319(13)	1.430
C2-C1-N2	120.25(9)	120.7	N2-C17	1.4700(13)	1.469
C6-C1-N2	120.29(9)	120.6	N3-C9	1.3282(13)	1.326
C5-C6-N1	115.03(9)	115.1	N3-N4	1.3756(11)	1.367
C1-C6-N1	126.46(9)	126.1	N4-C10	1.3521(13)	1.364
N1-C7-C8	126.62(9)	126.5	N4-C23	1.4439(13)	1.443
N1-C7-S1	119.42(8)	117.8	C8-C9	1.4188(14)	1.425

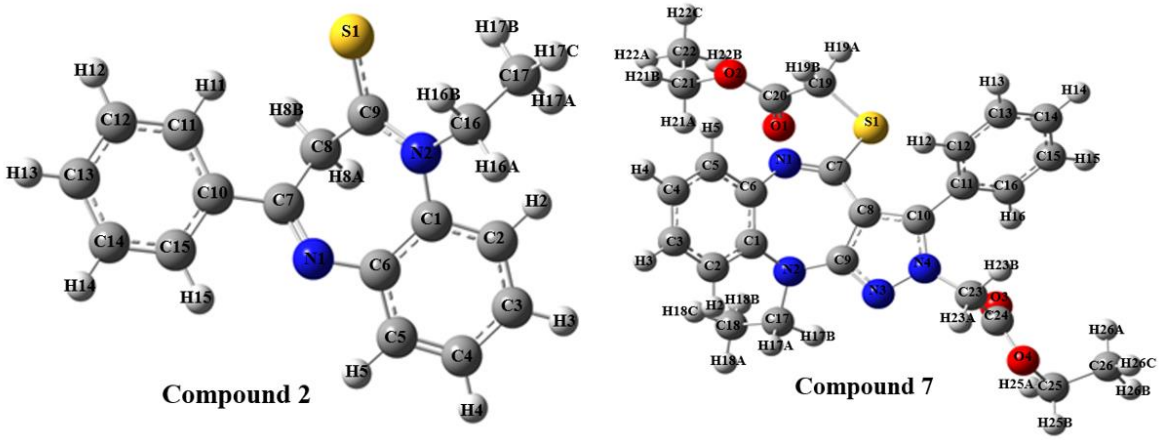

Figure 2. The optimized and ORTEP structures of compound **2** and compound 7.

2.3.2. Hirshfeld surface calculations

The Crystal Explorer 3.1 [53-57] program was used for the Hirshfeld surface analysis of compounds 2 and 7, and all the results obtained are presented in Figure 3-4. Here, cif* files of the structures were used to obtain the graphs of the structures. As shown in figures 2 and 4, there are three colors on the surface: red, blue and white. The dark red dots indicate strong hydrogen bonding points, the white dots indicate contacts close to the van der Waals separation, and the last blue dots indicate longer contacts [53-57]. The d_{norm} values were found as from -0.1142 to 1.3782 for compound **2** and from -0.2665 to 1.6826 for Compound **7**. Now, if we analyse for compounds **2** and **7** one by one; as seen from Figure 3 (a) the interaction distances of both S-H bonds were determined as 2.721Å and the contribution of inter-contacts to the Hirshfeld surfaces were obtained as H-H (55.2%), C-H/H-C (24.6%), S-H/H-S (11.6%) and N-H/H-N (4.7%) as seen from the (Figure 3 (b-e)), respectively.

On the other hand, as seen from Figure 4(a) the interaction distances of O-H and N-H bonds were determined as 2.254Å and 2.953Å, respectively. In addition, the contribution of internal contacts to the Hirshfeld surface is also obtained as H-H (53.6%), C-H/H-C (18.7%), O-H/H-O (16.5%), N-H/H-N (6.2%) and S-H/H-S (3.8%) as seen from the (Figure 4(b-f)), respectively.

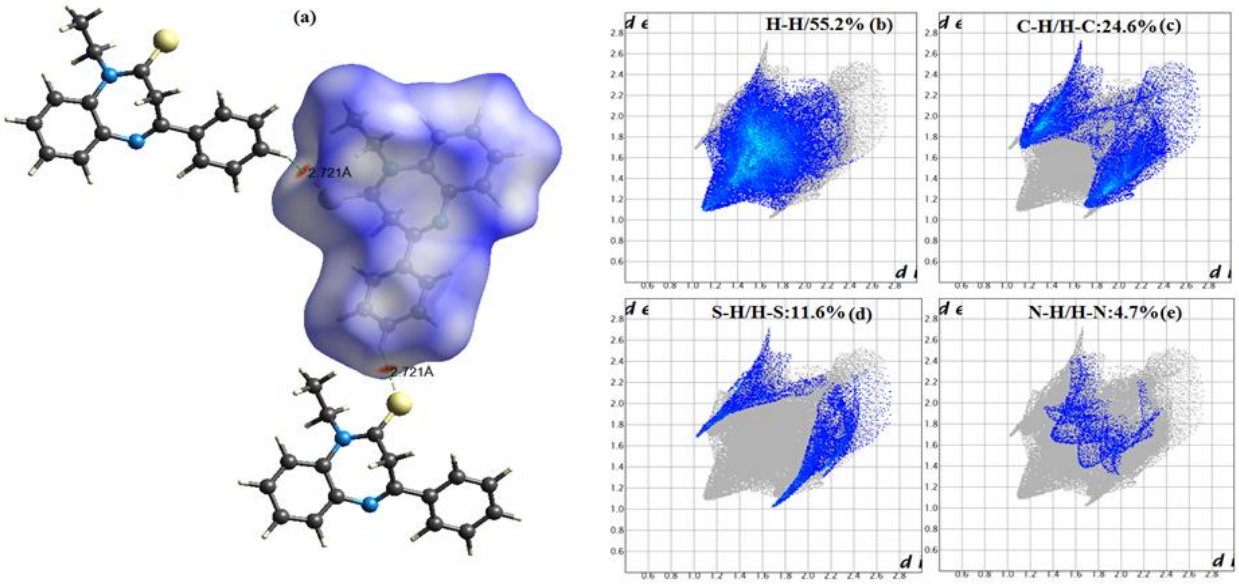

Figure 3. The 3D Hirshfeld surface (a) and 2D fingerprint histograms (b-e) of compound **2**.

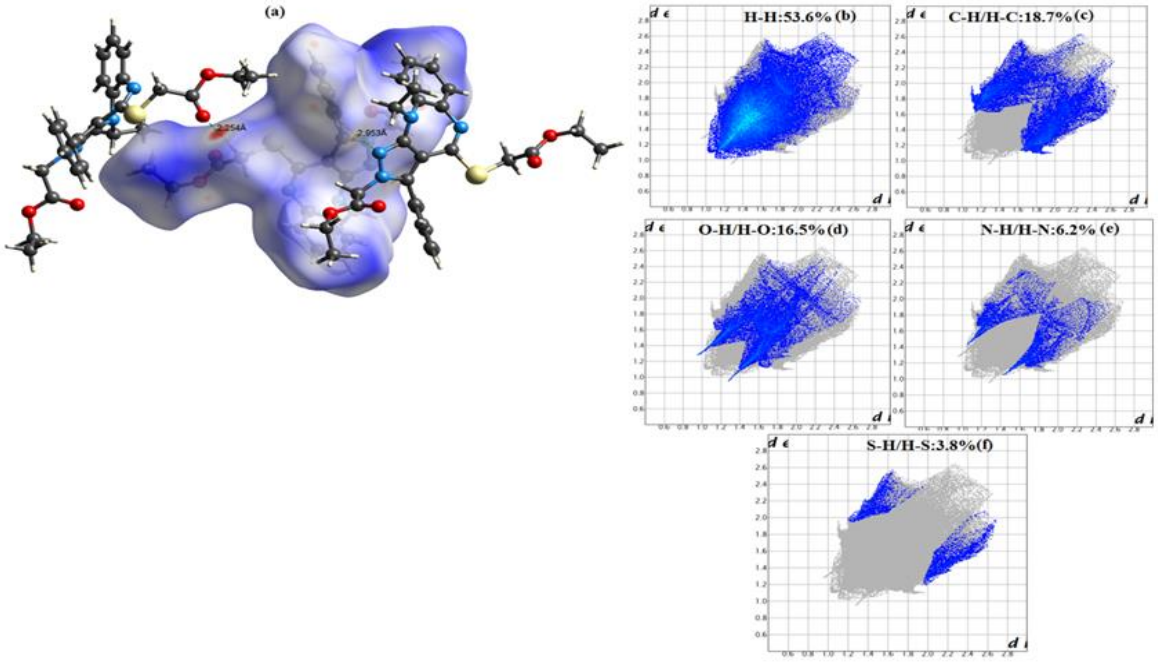

Figure 4. The 3D Hirshfeld surface (a) and 2D fingerprint histograms (b-f) of compound **7**.

2.3.3. HOMO-LUMO Analyses

The formation of the transition state of chemical reactivity according to the Frontier Molecular Orbital Theory (FMO) is due to the interaction between the frontier orbitals (HOMO and LUMO) of the reactive regions and this analysis is very important for theoretical organic chemistry. In this part, firstly compound **2** and **7** were optimized in chloroform solvent, then by using the obtained chk* file HOMO and LUMO distributions of the compound **2** and **7** were calculated with functional B3LYP and 6-31G(d,p) basis set.

The results for compound **2** and **7** were listed in Table 3 and also the distributions were shown in Figure 5. In this figure, positive phase is represented with the red color and the negative phase is with the green color. The LUMO is largely focused almost over the whole molecular moiety except C16-C17 parts whereas the region of HOMO spreads approximately over the benzodiazepine group (with S part) and partially over the C16, C17 and C1 (positive phase) atoms for compound **2**. When it comes to Compound **7**, The LUMO is largely focused almost over the whole molecular moiety except C24-C26, C19-C20-O2-C21-C22 parts whereas the region of HOMO spreads approximately all over the benzodiazepine group and S1 atom except with C11 benzene ring and O4-C25-C26, C19-O1-C20-O2-C21-C22 parts. In literature, the energy differences of HOMO and LUMO (ΔE gap) provides a measure for the stability of the compound, so the lower value of ΔE is related to the higher stability [58]. Additionally, if the HOMO-LUMO energy differences of a molecule are small, the electron distribution can be easily manipulated and the polarization is large, and when the energy differences are large, the electron distribution differs less and the polarization is low. As seen from the Table 3, the HOMO-LUMO energy gap ($|E_{HOMO}- E_{LUMO}|$) was calculated as 4.091 eV and 4.063 eV for compound **2** and **7**, respectively in the chloroform solvent. These results support the above-mentioned literature related to stability. Additionally, the other related descriptor was calculated and listed as in Table 3.

Table 3. HOMO and LUMO energy values and other related parameters of compound **2** and **7**.

Parameters (eV)	Compound 2	Compound 7
E_{LUMO} (eV)	-1.771	-1.238
E_{HOMO} (eV)	-5.862	-5.301
Energy bandgap $|E_{HOMO}- E_{LUMO}|$	4.091	4.063
Ionization potential ($I = -E_{HOMO}$)	5.862	5.301
Electron affinity ($A = -E_{LUMO}$)	1.771	1.238
Chemical hardness (h = (I-A)/2)	2.045	2.031
Chemical softness (z = 1/2h)	0.244	0.246
Electronegativity ($\chi = (I+A)/2$)	3.817	3.269
Chemical potential ($\mu = -(I+A)/2$)	-3.817	-3.269
Electrophilicity index ($w = \mu^2/2h$)	3.561	2.631
Sum of Electronic and zero point Energies (a.u)	-1164.873834	-1925.259890

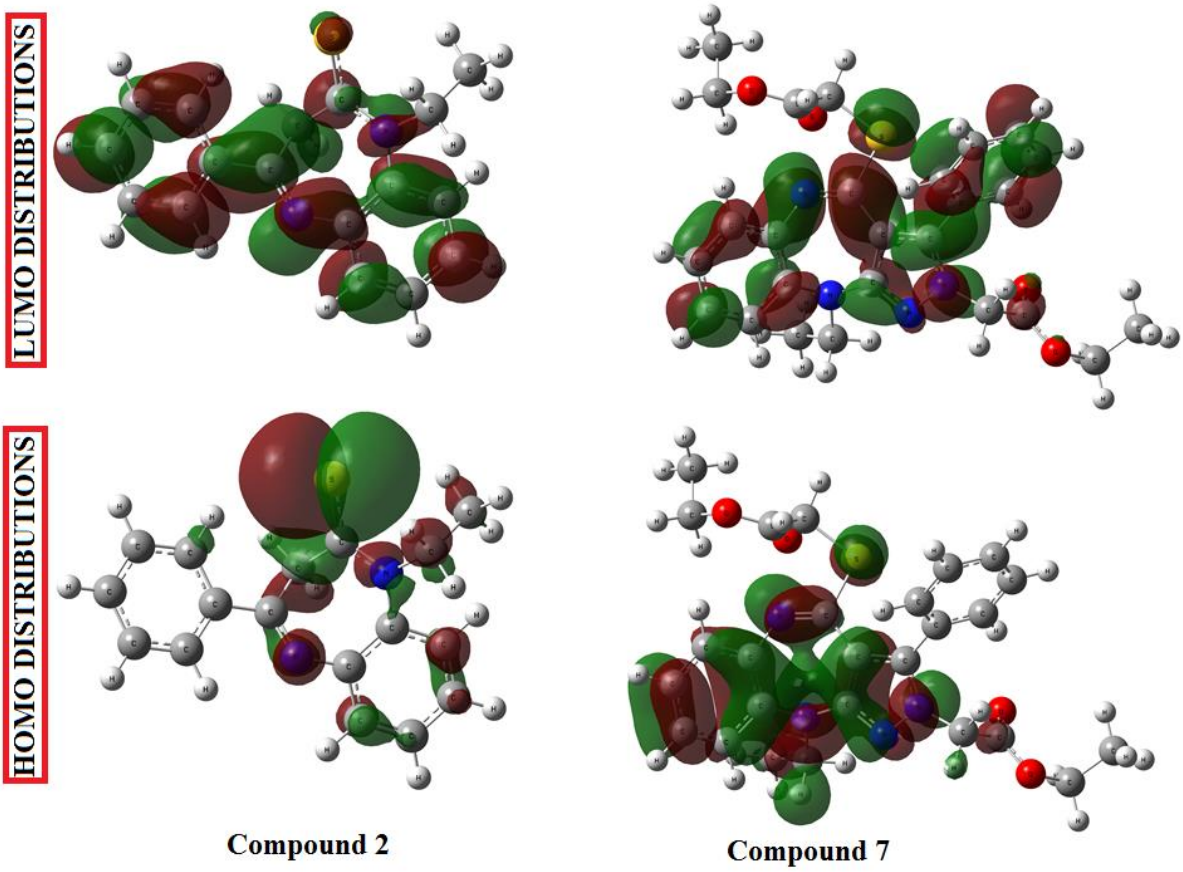

Figure 5. HOMO and LUMO plots of compound **2** and **7** with B3LYP/6-31G(d,p).

2.3.4. *NMR Analyses*

In this part, the experimental ^{1}H and ^{13}C NMR spectra of compound 2 and 7 were recorded in chloroform solution (Figure 2). To reinforce the experimental results, calculate the theoretical chemical displacements of ^{1}H NMR and ^{13}C NMR using the B3LYP function and 6-31G(d, p) bases. The IEFPCM model and the GIAO method are used after optimization of the same solvent [59-60]. The experimental and calculated NMR values were given in Table 4 and 5. The theoretical results were obtained by using $\delta^{x}_{iso}=\sigma^{TMS}_{iso}-\sigma^{x}_{iso}$ equation, here δ^{x}_{iso} is the isotropic chemical shift, σ^{x}_{iso} is the isotropic absolute shielding of the compound **2** and **7** and σ^{TMS}_{iso} is the isotropic absolute shielding of tetramethylsilane. From Table 4 and 5, we can conclude that there is very good consistency between the calculated and experimental chemical shifts of compound **2** and **7**.

Table 4. The experimental and computed ^{13}C and ^{1}H-NMR isotropic chemical shifts (with respect to TMS, all values in ppm) of compound **2.**

Atoms	Compound **2**-^{13}C-NMR		Atoms	Compound **2**-^{1}H-NMR	
	$\delta_{exp.}$	$\delta_{cal.}$		$\delta_{exp.}$	$\delta_{cal.}$
C1	128.87	128.78	H2	7.25- 8.5	8.00

C2	110,22-128,15	110.23	H3		7.67
C3		113.62	H4		7.77
C4		114.80	H5		7.76
C5		117.07	H8A	3.15	3.10
C6	139.84	132.16	H8B	4.17	4.77
C7	144.26	150.57	H11	7.25- 8.5	8.76
C8	35.99	41.15	H12		7.94
C9	192.93	185.55	H13		7.93
C10	110,22-128,15	125.00	H14		7.89
C11		117.73	H15		9.02
C12		116.64	H16A	4.12	3.87
C13		119.54	H16B		5.06
C14		116.42	H17A	1.15	1.27
C15		116.83	H17B		2.82
C16	44.26	47.67	H17C		1.67
C17	14.7	6.87			

Table 5. The experimental and computed ^{13}C and ^{1}H-NMR isotropic chemical shifts (with respect to TMS, all values in ppm) of compound **7.**

Atoms	Compound **7-**^{13}C-NMR		Atoms	Compound **7-**^{1}H-NMR	
	$\delta_{exp.}$	$\delta_{cal.}$		$\delta_{exp.}$	$\delta_{cal.}$
C1	142.17	130.04	H2	7.02- 7.14	7.21
C2	119.32	108.60	H3		7.41
C3	119.65	113.75	H4		7.36
C4	123.72	111.44	H5		7.28
C5	125.95	117.53	H12	7.37- 7.49	7.62
C6	142.42	131.68	H13		7.82
C7	158.46	154.57	H14		7.90
C8	109.12	100.58	H15		7.87
C9	160.85	151.14	H16		8.15
C10	143.56	134.97	H17A	3.75	3.90
C11	145.30	118.93	H17B		4.00
C12	128.37	119.64	H18A	1.35	1.70
C13	128.55	116.41	H18B		1.31
C14	128.63	118.06	H18C		1.11
C15	129.93	116.60	H19A	4.15	3.11
C16	130.36	118.07	H19B		3.82
C17	50.51	35.91	H21A	4.17	5.08
C18	13.01	5.99	H21B		4.00
C19	32.73	32.04	H22A	1.30	1.36
C20	169,42	157.21	H22B		1.68
C21	61.77	54.48	H22C		1.11
C22	14.08	8.13	H23A	4.54	4.66
C23	41.99	44.42	H23B		4.35
C24	167,60	157.43	H25A	4.20	4.18
C25	61.26	55.31	H25B		5.35
C26	14.18	7.91	H26A	1.25	1.45
			H26B		1.80
			H26C		1.27

2.3.5. *Molecular Docking Studies*

The goal of this part is to investigate the molecular docking between compound 2 and 7 ligands and CYP2C19 protein: 4GQS (PDB code) [61]. The CYP2C19 which is a vital member of cytochrome P-450 enzyme superfamily and has a very important role in drug metabolism [62]. Before docking, it is necessary to delete all-natural ligands attached to receptor molecule to clear the active site for more efficient calculations. First, the PDB and PDBQT forms of the ligand (compounds 2 and 7 optimized with B3LYP / 6-31G (d, p)) And the protein receptor is prepared by Discover Studio Visualizer 4.0 software (DSV 4.0) [63]. Then active sites of 4GQS protein were determined as GLY437, VAL436, CYS435, ARG433, SER429, PHE428, PRO427, HIS368, LEU366, SER365, ILE362, ARG335, VAL331, THR305, THR302, THR301, GLU300, GLY298, ALA297, ASP293, PHE226, ASN218, ILE215, GLN214, VAL208, ILE205, ARG124, TRP120, PHE114, ILE112, ARG97 and ILE42 residues and the grid boxes were determined according to the these active residues: 70x78x80 $Å^3$, spacing=0.375 and x, y, z centers: -70.672, 19.218 and -42.74. Therefore, between compound **2**+4GQS and compound **7**+4GQS molecular docking interactions were given at Table 6 and the obtained 2D and 3D forms were depicted in Figure 6 and 7, respectively. From the Table 6 and Figure 6 and 7, it can be said that the best docking result occurs between compound **7** and 4GQS with -7.9 kcal/mol binding energy, 1.61904 μM inhibition constant and four conventional hydrogen bonding. Here, the inhibition constants (Ki) for each conformer were computed from $K_i = \exp(\Delta G/RT)$ equation, where ΔG, R and T are respectively the docking energy, the gas constant (1.9872036×10^{-3} kcal / mol) and the ambient temperature (298.15 K). As a result, from in silico based molecular docking scores support that compound **2** and **7** ligands are potent 4GQS protein inhibitors. The obtained all docking results and bonding types could be seen clearly from the Figure 6, 7 and 8, respectively.

Table 6. Binding affinity and RMSD results for 4GQS inhibitors of compounds 2 and 7 in different positions.

Mode	Compound **2**-4GQS				Compound **7**-4GQS			
	Affinity (kcal/mol)	rmsdl.b.	rmsdu.b.	Inhibition Constants (μM)	Affinity (kcal/mol)	rmsdl.b.	rmsdu.b.	Inhibition Constants (μM)
1	-7.6	0.000	0.000	2.68633	-7.9	0.000	0.000	1.61904
2	-7.0	17.164	21.001	7.39542	-7.6	2.213	3.295	2.68633
3	-6.7	17.593	20.503	12.2706	-6.2	2.481	6.092	28.5343
4	-6.7	31.303	32.310	12.2706	-6.1	2.647	5.753	33.7806

5	-6.6	20.566	23.812	14.5266	-5.8	3.756	6.598	56.0492
6	-6.4	2.895	6.679	20.3594	-5.8	24.549	8.591	56.0492
7	-6.4	2.523	3.436	20.3594	-5.8	24.548	8.782	56.0492
8	-6.2	27.771	29.654	28.5343	-5.6	24.861	7.683	78.5543
9	-6.1	20.891	22.988	33.7806	-5.6	25.010	6.840	78.5543
10	-6.1	14.167	15.645	33.7806	-5.5	3.827	7.646	92.9974

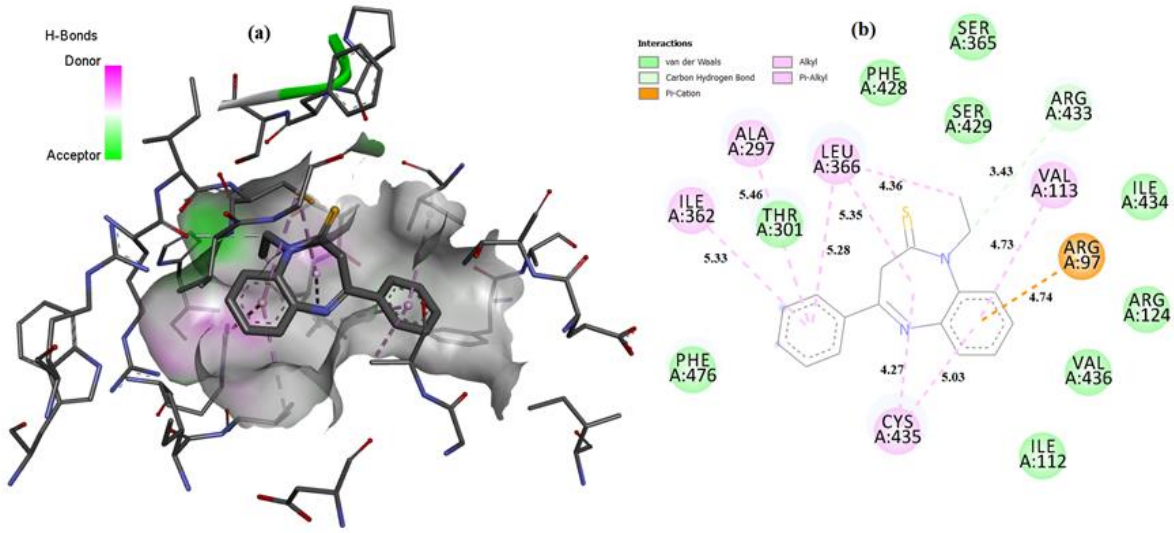

Figure 6. The molecular docking results of compound **2** with 4GQS protein, 2D forms (a) and 3D forms (b).

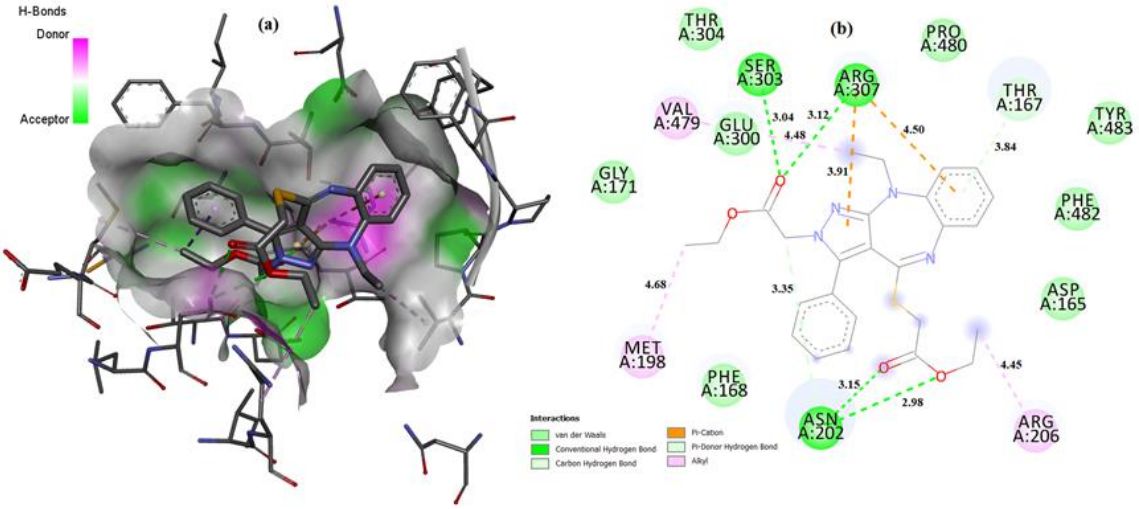

Figure 7. The molecular docking results of compound **7** with 4GQS protein, 2D forms (a) and 3D forms (b).

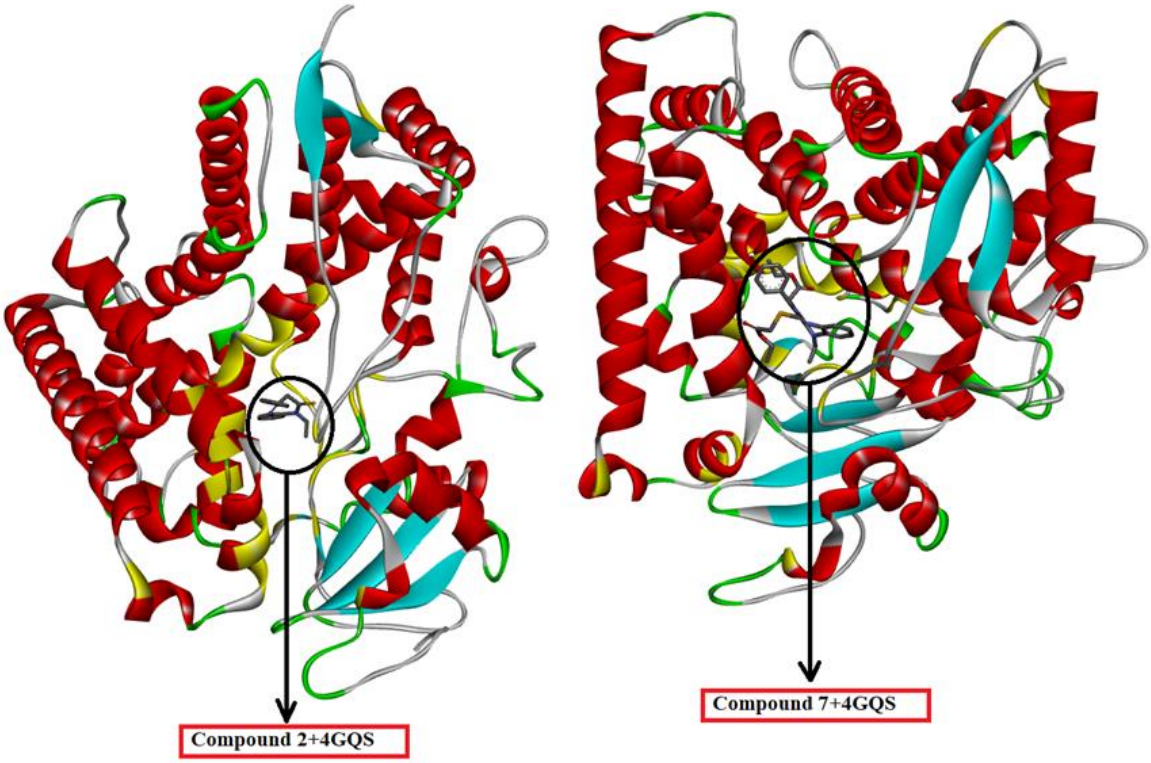

Figure 8. The three-dimensional structure of 4GQS protein with the title molecules **2** and **7**.

2.*4. Inhibiting tendency against metallic corrosion*

As the inhibition of corrosion using organic compounds is largely attributed to their adsorption on the metal surface [64], it is important to examine the affinity of the newly synthesized derivatives to interact with the surface of selected metals (i.e. Fe, Cu and Al). For this, the Monte Carlo simulations were performed employing universal as the force field by considering the periodic boundary conditions [65, 67]. It is well known that in acidic solutions the surface of pure metals is almost clean without the presence of oxide form. Accordingly, the simulations were carried out on Fe(110), Cu(111) and Al(111) surfaces [68, 69]. Five layers with similar surficial density (i.e. number of atoms per layer) of these surfaces with 60 Å as a vacuum region were used to build the suitable box of simulations. Concerning the electrostatic and Van der Waals energetic components, they were calculated using Ewald and atom-based summation approaches, respectively. As the acidic environment is considered in this prediction study, the protonated form of these compounds (noted as C2-H and C7-H) was also treated. On the other hand, the current simulations were extended to study also the affinity of the water molecule and H_3O^+ ion to be adsorbed onto selected metallic substrates, which are the principal constituents of acidic solutions. In this work, the binding energy ($E_{Binding}$) of different compounds is calculated according to the following expression:

$$E_{Binding} = \left(E_{Metal\ surface} + E_{ads}^{Comp}\right) - E_{Total} = -E_{ads} \quad (1)$$

Where E_T, E_{Surf} and E_{ads}^{Comp} represent the energy of the whole system, metal surface, adsorbed compound, while E_{ads} is the adsorption energy. All listed calculations in this section were performed employing Materials Studio 6.0 software.

To investigate the probable interfacial interactions of developed compounds in their neutral and protonated forms with the iron, copper and aluminum surfaces, the *Monte Carlo* simulations were conducted. The calculated binding energies for different compound/surface systems are depicted in Figure 9. It is evident from calculated values ($E_{binding} = -E_{ads}$) that studied derivatives could be adsorbed spontaneously onto all selected metallic surfaces [70]. Furthermore, for neutral and protonated forms, the binding energy was found to increase as follows: compound **7** > compound **2**. This indicates the great tendency of compound **7** to interact with studied metal surfaces rather than compound **2**. Such a trend can be attributed to the presence of more favorable sites of adsorption in compound **7** (i.e. heteroatoms and π-electrons) as compared to compound **2** [71]. Considering the binding energy/inhibition efficiency linear relationship [72], for all considered metals, the expected inhibition effectiveness toward corrosion of these compounds can be ranked as compound **7** > compound **2**. Besides, we can note that the calculated $E_{binding}$ depends on the chemical nature of the metal surface, which is ranked as Al(111) >> Fe(110) > Cu(111) for the same compound. These finding outlines that the anticipated inhibition effectiveness of a given compound will be reduced in the same ranking. In other words, the developed derivatives can doubtless act as good inhibitors against aluminum corrosion as compared to other studied metal in this work.

To get a credible vision on the ability of these compounds to protect metal toward corrosion, it is important to consider further the adsorption affinity of the constituents of aggressive media i.e. acidic solution. In this regard, the interfacial interactions of a water molecule and H_3O^+ ion with metal surfaces should be taken in our case. The calculated $E_{binding}$ of water molecule and H_3O^+ ion on the studied surfaces are graphically presented in Figure 9. According to the illustrated data, H_2O and H_3O^+ species can adsorb spontaneously on the chosen metal surfaces. By comparing their affinity to interact with the metal surface and corresponding ones for investigating organic compounds; it is clear that H_2O shows a lower affinity meaning the capacity of the synthesized compounds to replace pre-adsorbed water molecules onto all considered metal surfaces. Nevertheless, H_3O^+ specie was exhibited a great tendency to interact with Fe(110) and Cu(111) surfaces in comparison

with the synthesized compounds, which outlines the competitive effect at the metal/solution interface leading to lower inhibition property of these compounds for iron and copper metal in acid media. The opposite behavior is observed in the case of Al(111) from which the developed derivatives have a significant priority to adsorb onto the aluminum surface. Hence, these derivatives can show the enhanced capacity to control the aluminum corrosion in acid solution as compared to iron and copper metals.

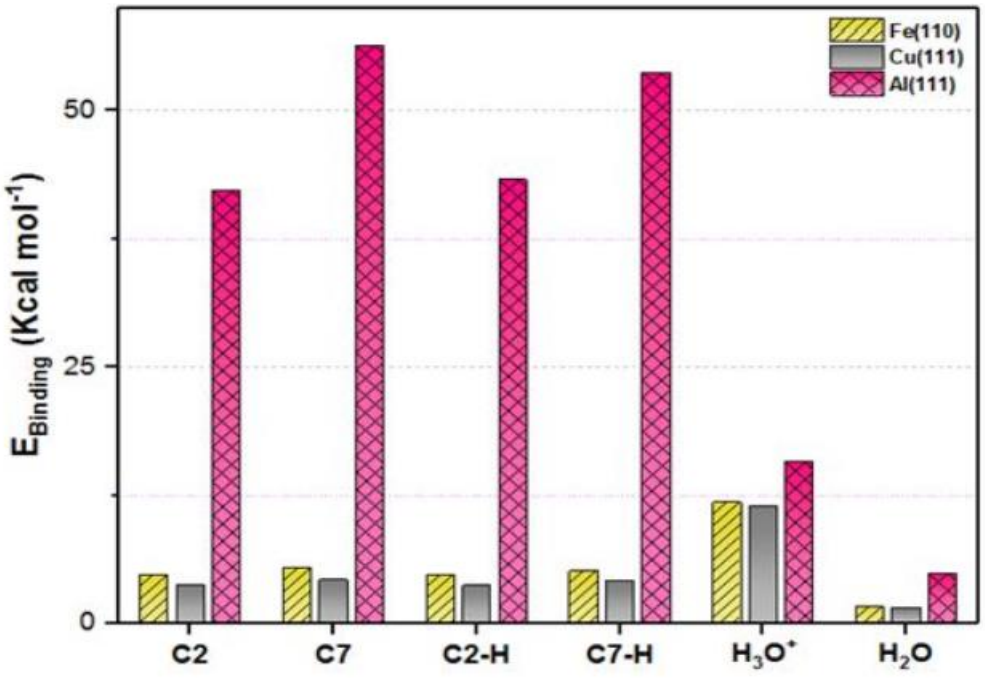

Figure 9. Binding energy of the newly synthesized compounds **2** and **7**, as well as a water molecule and H_3O^+ ion, onto Al(111) surface.

Further to the energetic aspect (i.e. $E_{binding}$), it is also needed to study the adsorption process of these compounds from a geometrical side. As good inhibition effectiveness is expected for the aluminum, we are limited in **Figure 10** to present a more stable adsorption configuration of these derivatives in their neutral (C**2** and C**7**) and protonated (C**2**-H and C**7**-H) forms on the Al(111) surfaces. It can be seen in the last figure that the investigated organic compounds in both protonation forms are closely placed on the Al(111) surface, which reveals their adsorption. In this configuration, we can note the parallel adsorption geometry of the benzodiazepine moiety for both derivatives. Whereas, the extra-substituents are either parallel or directed away from the Al(111) surface as can be noted for C**7** and C**7**-H molecules, respectively. In this regard, the parallel orientation can offer better coverage of the aluminum surface that increases by rising molecular volume of the derivative (i.e. compound **7** > compound **2**). These findings underline the capacity of these compounds to effectively protect aluminum toward corrosion in the following order:

compound **7** > compound **2**, which confirms further the energetic analysis of the adsorption process.

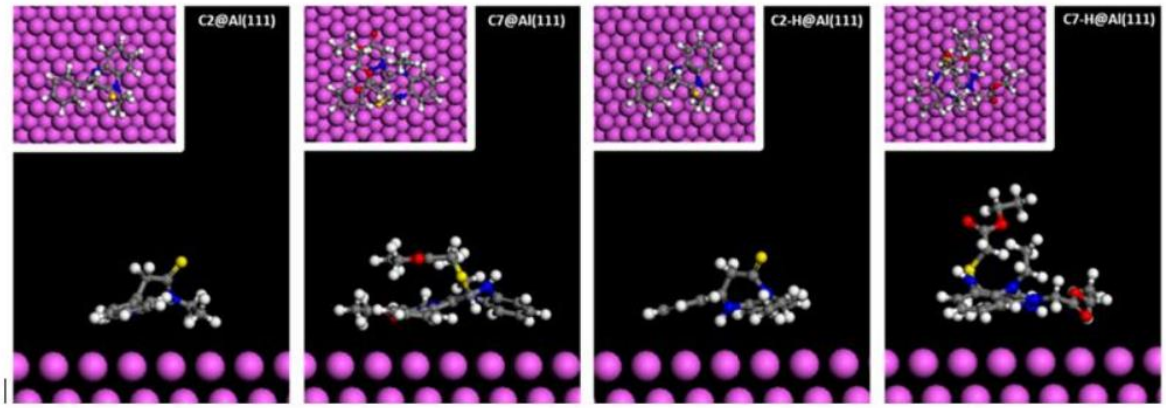

Figure 10. Side and top (above-left) views of the more stable adsorption configuration of the newly synthesized derivatives in their neutral (C**2** and C**7**) and protonated (C**2**-H and C**7**-H) forms onto the Al(111) surfaces.

2.5. *Antibacterial activity*

In order to compare and analyze the antibacterial properties provided by the compounds (**2-7**) and commercially available antibiotics such as chloramphenicol (Chlor) and ampicillin (Amp), we tested the following strains of *Staphylococcus aureus (ATCC-25923) , Escherichia coli (ATTC-25922), Pseudomonas aeruginosa (ATCC-27853) and Streptococcus (ATCC-29212)*, the applicability of compounds (**1-7**) as antibacterial agents was evaluated by the disc diffusion method [73,76]. Figure 11 summarizes the inhibition diameter (mm) values of compounds (**1-7**) and the commercially available antibiotics Chlor and Amp. The disc diffusion test is used to determine the MIC of synthesized derivatives of [1,5]benzodiazepines (**1-7**). The results of the antibacterial activity of the tested compound **2** obtained by sulfurization of 1-éthyl 4-phényl -1,5-benzodiazépin-2-one **1** with phosphorus pentasulfide (P_2S_5) resulted in anti-bacterial activity is increase of **MIC** = 15µg/mL for *Escherichia coli* and *Streptococcus fasciens*, 7,5 for *Staphylococcus aureus* and **MIC** = 3,75µg/mL for *Pseudomonas aeruginosa*. Moreover, in order to increase the inhibitory activity of pyrazolo [1,5] benzodiazépine-4-thione **3** has been via reaction hydrazine by compound **2**. the (5)-N-[methyl(ethyl)-2-aminophenylamino-5(3)-phenylpyrazole **3** showed a similar better activity against the two bacterial strains as that tested by compound **3**, with a MIC of 3,75 µg/mL for *Pseudomonas aeruginosa*, *Staphylococcus aureus*, MIC = 7,5 µg/mL for *Escherichia coli*, and 30µg/mL for *Streptococcus fasciens*. However, compound **3** with carbon disulfide in the presence of pyridine, demonstrated a decrease activity with an MIC of 30 µg/mL for *Escherichia coli*,

Pseudomonas aeruginosa, and Streptococcus fasciens, and **7,5** µg/mL for *Staphylococcus aureus*. Indeed, among the 3 alkylated products **5**, **6** and **7**, the compound **7** which has showed a better activity, with a MIC of **3,75** µg / mL for *Escherichia coli* and **7,5** µg / mL for *Staphylococcus aureus* and **15** µg / mL for *Pseudomonas aeruginosa*, and *Streptococcus fasciens*. In particular, derivatives functionalized by ester groups and benzene rings have the strongest antibacterial activity (92% of pathogenic bacteria are sensitive to these compounds). Studies such as antifungal, anti-inflammatory, anti-cancer and anti-parasitic tests must also be conducted, as the literature shows that these subjects have many interesting results. Other bacteria should also be tested to extend this research.

The results are presented in the form of antibiograms below:

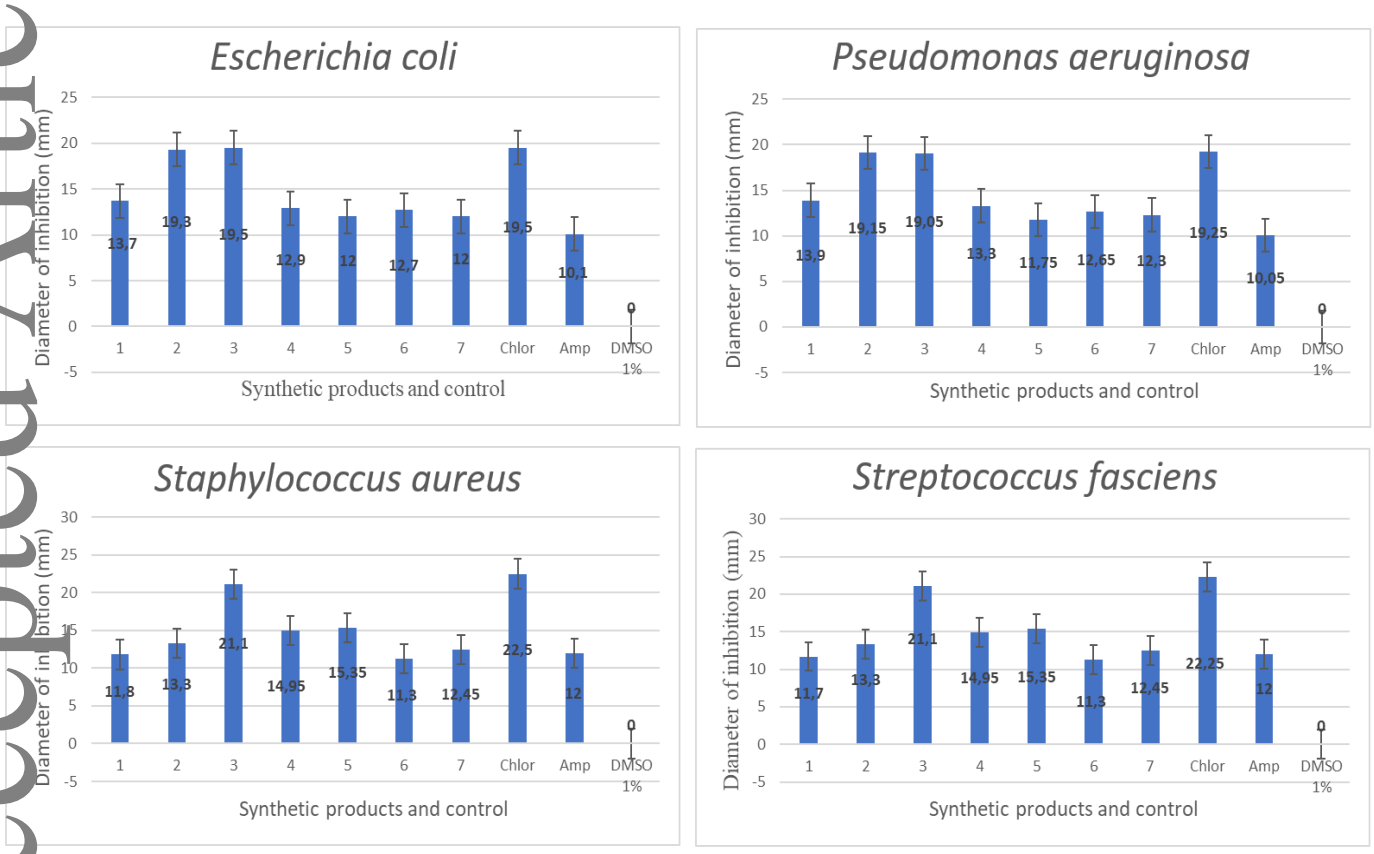

Figure 11. The figure below summarizes the antibacterial activity of the synthesized compounds (1-7) against the bacteria tested (*E. coli*, *Pseudomonas aeruginosa*, *Staphylococcus aureus and Streptococcus*). Chlorine, chloramphenicol (30 µg / mL); Ampere, ampicillin (10 µg / mL); DMSO, dimethylsulfoxide (1%).

Table 7: Antibacterial activity of the compounds (**1-7**) represented as Minimum Inhibitory Concentration [MIC (µg/mL)]

	MIC (µg/mL)			
	E. coli	***P. aeruginosa***	***S. aueus***	***S. fasciens***
1	30	7,5	30	3,75
2	15	3,75	7,5	15

3	7,5	3,75	3,75	30
4	30	30	7,5	30
5	7,5	30	30	3,75
6	30	30	30	30
7	3,75	15	7,5	15
Chlor	6.25	6.25	12.5	3.75

3 | EXPERIMENTAL SECTION

3.1. General

The spectroscopic characterizations of the synthesized compounds (**2-7**) were achieved by recording NMR spectra: ^{1}H-NMR (300 MHz) and ^{13}C-NMR (75 MHz), respectively, which were measured on a Bruker Avance DPX 300 instrument. Thin-layer chromatography (TLC) and column chromatography were carried out on silica plates (Merck 60 F254) and silica gel (Merck 60, 230-400 mesh) respectively. Melting points of compounds **2-7** were determined in open capillaries. The chemical shifts (δ) were expressed in ppm and the coupling constants (J) in Hertz (Hz), downfield from TMS [tetramethylsilane, $Si(CH_3)_4$] which has been assigned a chemical shift of zero, TMS as an internal reference.

3.2. Procedure of Synthesis compound 2

To a solution of 1-ethyl-4-phenyl-1,5-benzodiazepin-2-one **1** (0.80 g, 3.04 mmol) in 20 ml of pyridine was added phosphorus pentasulfide (0.84 g, 3.65 mmol). The mixture was refluxed for 4 h. After cooling, the solvent was evaporated under reduced pressure. The residue formed was washed with hot water [77]. The compound obtained was crystallized from ethanol to afford crystals of the title compound.

***Compound* 2: Yield** (%)= 80; mp = 345K; **^{1}HNMR (300 MHz, $CDCl_3$)**: 1.15 (t, *J*=7,14Hz, 3H); 3.15 (d, *J* =12Hz, 1H); 4.2 (q, *J* =7.14Hz 2H); 4.7 (d, *J* =12Hz, 1H); 7.25-8.5 (m, 9H); **^{13}C**NMR **(75 MHz, $CDCl_3$):** 14.17 (CH_3); 35.99 (CH_2); 44.26 (NCH_2); 110.22-128.15(CHar); 128.87(Car); 139.84(Car); 141.18 (Car); 144.26 (C=N); 192.93 (C=S).

3.3. Procedure of Synthesis compound 3

Dissolve 0.01 mole of 1-ethyl-4-phenyl-1,5-benzodiazepine-2-thione **2** in 40 ml of ethanol and add one equivalent (or excess) of hydrazine hydrate. The mixture was stirred at room temperature for 48 hours. After cooling, the solvent was concentrated under reduced pressure, and the residue obtained was chromatographed on a silica gel column using a ((90/10) hexane / ethyl acetate eluent).

***Compound* 3: Yield** (%) = 35; mp = 423K; **^{1}H NMR** (**300 MHz, $CDCl_3$**): 1.23 (t, *J* = 7.0 Hz, 3H); 3.53 (q, *J* = 7 Hz, 2H); 5.62 (s, 1H); 5.90 (m, 2H); 7.12-7.54 (m, 9H). ^{13}C NMR

(75 MHz, $CDCl_3$): 13.60 (CH_3); 41.80 (CH_2); 98.48 (CH); 124.74-129.62 (CHar); 108.84, 125.43, 126.31, 149.87(Car); 150.51 (C=N).

3.4. Synthesis procedure of compound 4:

To a solution of 0.01 mol of 3- [N-2- (aminophenyl) N-ethylamino] -5-phenylpyrazole **3** solubilized in a minimum of pyridine, were added 20 ml of carbon disulfide. The mixture reaction was left under magnetic stirring at room temperature overnight. The yellow precipitate formed was filtered and recrystallized from ethanol.

Compound 4: Yield (%) = 85; mp = 553K; **^{1}H NMR (300 MHz, DMSO-d_6)**: 1.25 (t, *J* = 6.9 Hz, 3H); 3.75 (q, *J* = 6.9 Hz, 2H); 7.13–7.71 (m, 9H); 11.24 (s, 1H, NH); 12.97 (s, 1H, NH). **^{13}C**NMR **(75 MHz, DMSO-d_6):** 13.60 (CH_3); 40.09 (CH_2); 119.76(C_3), 123.92-136.57(CHar); 136.57-150.02(Car), 192.78 (C=S) (see figures *S1-S2 (Supporting Information: spectrum ^{1}H and ^{13}H NMR for Compound **4B**)*.

3.5. ***General procedure of synthesis compounds 5-7:***

To a solution of 0.01 mol of 10-ethyl-3-phenylpyrazolo[4,3-c][1,5]benzodiazepine-4-thione **4** in 60 ml of dimethylformamide were added 0.02 mol of alkylating agent : (propargyl bromide, benzyl chloride or ethyl bromoacetate) and 0.02 mol of K_2CO_3 and 0.001 mol of tetra-n-butylammonium bromide (TBAB). The mixture was stirred at room temperature for 24 hours. After filtration of potassium carbonate and evaporation of dimethylformamide in reduced pressure, the residue obtained was chromatographed on a silica column (eluent: ethyl acetate / hexane 30:70).

***Compound* 5: Yield** (%) = 75; mp = 404 K; **^{1}H NMR (300 MHz, DMSO-d_6)**: 1.22 (t, 3H, *J* = 7Hz, CH_3); 3.04 (t, 1H, *J* = 2.7Hz, *H*CCH_2S); 3.37 (t, 1H, *J* = 2.7Hz, *H*CCH_2N); 3.68 (q, 2H, *J* = 7Hz, CH_2); 3.79 (d, 2H, *J* = 2.7Hz, S*C*H_2C≡C); 4.64 (d, 2H, *J* = 2.7Hz, NCH_2CC); 7.02-7.55 (m, 9Har). **^{13}C** NMR **(75 MHz, DMSO-d_6):** 12.88 (CH_3); 17.51 (CH_2); 33.15 (CH_2); 41.23 (CH_2); 73.11 (CH); 76.02 (CH); 78.18 (Cq); 79.94 (Cq); 119.23-130.07 (CHar); 142.09-159.99 (Car) (see figures *S3-S4 (Supporting Information: spectrum ^{1}H and ^{13}H NMR for Compound **5**)*.

Compound 6: Yield (%) = 60; mp = 408K; **^{1}H NMR (300 MHz, DMSO-d_6)**: 1.20 (t, *J* = 7.2 Hz, 3H, CH_3); 3.63 (q, 2H, *J* = 7.2 Hz , CH_2); 4.19 (s, 2H, SCH_2); 5.03 (s, 2H, NCH_2); 6.94-7.47 (m, 19CH_{ar}), **^{13}C** NMR **(75 MHz, DMSO-d_6):** 12.94 (CH_3); 33.28 (CH_2); 41.23 (CH_2); 51.79 (CH_2); 119.76-137.92 (CHar); 144.72-159.84 (Car, C3', C5') (see figures S5-S6 (Supporting Information: spectrum ^{1}H and ^{13}H NMR for Compound **6**).

Compound 7: Yield (%) = 60; mp= 419K; **^{1}H NMR (300 MHz, $CDCl_3$)**: 1.25 (t, 3H, CH_3); 1.30 (t, 3H, CH_3); 1.35 (t, 3H, CH_3); 3.75 (q, 2H, CH_2); 4.17 (q, 2H, CH_2); 4.20 (q, 2H,

CH_2); 4.15 (s, 2H, SCH_2); 4.54 (s, 2H, NCH_2); 7.02-7.50 (m, 9Har). **^{13}C NMR (75 MHz, $CDCl_3$):** 13.01 (CH_3); 14.08 (CH_3); 14.18 (CH_3); 32.73 (CH_2); 41.99 (CH_2); 50.51 (CH_2); 61.26 (CH_2); 61.77 (CH_2); 119.32 -130.36 (CHar); 142.09-160.85 (Car, C3 ', C5'); 167,60 (C=O); 169,42(C=0) (see figures S7-S8 (Supporting Information: spectrum ^{1}H and ^{13}H NMR for Compound **7**).

4/ CONCLUSIONS

The studies carried out in the framework of this work show that the 1,5-benzodiazepine fraction constitutes an interesting scaffolding, present in several drugs and natural products. In addition, we report the synthesis of new 1,5-benzodiazepine derivatives (**2-7**). Their structure has been elucidated using X-ray crystallography and spectroscopy techniques. By specifically showing that the alkyl group is connected to the sulfur atom and the pyrazole nitrogen atom in position 2 instead of position 1 of the tricyclic compound as described in the literature, we have confirmed the structure of pyrazolodiazepine **5-7**. The theoretical method used allows to reproduce the X-ray geometrical parameters, spectral data and chemical displacements of ^{1}H and ^{13}C NMR. Hirshfeld surface analysis was used to confirm the presence of intermolecular interactions in compounds **2-7**. The use of quantum chemistry DFT and in silico based molecular docking studies can reproduce the experimental spectral data well. The Monte Carlo simulation's outcomes reveal the ability of these derivatives to act as good corrosion inhibitors for aluminum in acid media as compared to iron and copper metals, in which the anticipated inhibition prevention order is compound **7** > compound **2**. The 1,5-benzodiazepine derivatives **2-7** exhibited antibacterial activity and could act as potent antibacterial agents.

Conflicts of interest

There are no conflicts to declare.

Acknowledgment

Researchers Supporting Project number (RSP-2020/78), King Saud University, Riyadh, Saudi Arabia, Authors would like to thank Prof. Dr. Fatih Ucun for his helpful contribution and Gaussian Calculations and JTM thanks Tulane University for support of the Tulane Crystallography Laboratory.

Abbreviations

Chlor-Chloramphenicol;

Amp-Ampicillin;

DMSO-dimethylsulfoxyde

MIC-Minimum Inhibitor Concentration

BHI-Brain heart infusion

HOMO-highest occupied molecular orbital

LUMO-lowest unoccupied molecular orbital

DSV 4.0-Discover Studio Visualizer 4.0

References

[1] Y. Filali Baba, Y. Sert, Y. Kandri Rodi, S. Hayani, J. T. Mague, D. Prim, J. Marrot, F. Ouazzani Chahdi, N. K. Sebbar, E. M. Essassi., J. Mol. Struct., **2019**, 1188, 255-268.

[2] S. Lahmidi, E. H. Anouar, L. El Hamdaoui, Y. Ouzidan, M. Kaur, J. P. Jasinski, N. K. Sebbar, E. M. Essassi, M. El Moussaouiti, J. Mol. Struct., **2019**, 1191, 66-75.

[3] M.A. Pasha and V.P. Jayashankar, Indian J. Chem., **2006**, 45B, 2716-2719.

[4] K.S. Atwal, J.L Bergey, and A. Hedberg, J. Med. Chem., **1987**, 30.4, 635-640.

[5] E.M. Rakib, M. Benchidmi, E.M. Essassi, Y. Kandri Rodi, J. Bellanet L. Lopez. Bull. Soc. Chim. Belg., **1996**, 105, 345.

[6] S. A. Majid, W. A. Khanday, R. Tomar, J. Biomed Biotechnol, **2012**, 2012, 1–6. doi:10.1155/2012/510650

[7] *Y. An, Z. Hao, X. Zhang, L. Wang,* Chem. Biol. Drug Des, **2016**, 88(1), 110–121. *doi:10.1111/cbdd.12739.*

[8] K. Chkirate, N. K. Sebbar, K. Karrouchi, & E. M. Essassi, J. Mar. Chim. Heterocycl., **2018**, 17, 1–27.

[9] A. Misra, *S. Jain, D. Kishore, V. Dave, K. R. Reddy, V. Sadhu, S. Sharma*, J. Microbiol. Methods, **2019**, 163,. *doi:10.1016/j.mimet.2019.105648*. 105648

[10] *A. H. Jadhav, H. Kim,* RSC Advances, 2013, 3(15), 5131. *doi:10.1039/c3ra22663h.*

[11] S. Gupta, C. Ameta, P. B. Punjabi, J. Heterocycl. Chem 57(6):2410 2427. https://doi.org/10.1002/jhet.3957.

[12] J. R. de Baun, F. M. Pallos, and D. R. Baker, U.S. Patent No. 3,947,475. 30 Mar., **1976**.

[13] J. R. de Baun, F. M. Pallos, and D. R. Baker, Chemical Abstracts., **1977**, 86, 5498d.

[14] J. K. Landquist, Comprehensive Heterocyclic Chemistry, Pergamon, Oxford, UK, 1., **1984**.

[15] L. O. Randall and B. Kappel, S. Garattini and E. Mussini, Eds., Raven, New York, NY, USA., **1973**. 27-51.

[16] G. Roma, G. C. Grossi, M. Di Braccio, M. Ghia, F. Mattioli, Eur. J. Med. Chem., **1991**, 26.5, 489-496.

[17] R. G. Kalkhambkar, G. M. Kulkarni, C. M. Kamanavalli, N. Premkumar, Asdaq, S. M. & C. M. Sun, Eur. J. Med. Chem. **2008**, 43(10), 2178-2188.

[18] R. Kumar and Y.C.Joshi. Arkivoc. **2007**, 13, 142-149.

[19] A. M. El-Sayed, H. Abdel-Ghany, and A. M. M. El-Saghier, Synth. Commun. **1999**, 29(20), 3561-3572.

[20] J. X. Xu, H. T. Wu, and S. Jin, Chin. J. Chem., **1999**, 17.1, 84-91.

[21] X. Y. Zhang, J. X. Xu, and S. Jin, Chin. J. Chem., **1999**, 4, 404-410.

[22] K. Kim, S. K. Volkman, and J. A. Ellman, J. Brazil. Chem. Soc ., **1998**, 9.4, 375-379.

[23] N. Hamou Ahabchane, S. Ibrahimi, M. Salem, E. M. Essassi, S. Amzazi, A. Benjouad, C. R. Acad. Sci. Paris, Chimie / Chemistry. **2001**, 4, 917–924.

[24] G. A.Archer et L.H.Sternbach. Chem. Rev ., **1968**, 68.6, 747-784.

[25] J. Knabe, H. P. Buech et S. Bender, Archiv der Pharmazie., **1995**, 328.1, 59-66.

[26] K. S. Atmal, J. L. Bergey, A. Hedberg et S. Moreland, J. Med. Chem, **1987**, 30(4), 635-640.

[27] V. Merluzzi, K. D. Hargrave, M. Labadia, K. Grozinger, M. Skoog, J. C. Wu, C. K. Shih, K. Eckner, S. Hattox, J. Adams, A. S. Rosenthal, R. Faanes, R. J. Eckner, R. A. Koup et J. L. Sullivan, Science., **1990**, 250.4986, 1411-1413.

[28] B. D. Puodziunaite, R. Janciene, L. Kosychova, & Z. Stumbreviciute, Arkivoc., **2000**, 4, 512-522.

[29] M. Di Braccio, G. Grossi, G. Roma, L. Vargiu, M. Mura, Eur. J. Med. Chem, **2001**, 36, 935-949.
[30] D. A. Claremon, N. Liverton, H. G. Selnick, & G. R Smith, PCT Int. Appl. WO 9640653., **1996**.
[31] M. E. Tranquillini, P. G. Cassara, M. Corsi, G. Curotto, D. Donati, G. Finizia, G. Pentassuglia, S. Polonelli, G. Tarzia, A. Ursini and F. Van Amsterdam, Archiv der Pharmazie. **1997**, 330.1, 353-357.
[32] W. Werner, J. Baumgart, G. Burckhardt, W.F. Fleck, K. Geller, W. Gutsche, H. Hanschmann, A. Messerschmidt et W. Roemer, Biophys Chem., **1990**, 35(2-3), 271-285.
[33] A. Ursini, A. M. Capelli, P. Cassarà, et all. J. Med. Chem., **2000**, 43.20, 3596-3613.
[34] B. Djerrari, E.M.Essassi, J.Fifani, B.Garrigues, M.Pierro. Indian. J. Chem. **2003**, 42B, 2820.
[35] D. J. Lauffer et M. D. Mullican, Bioorg. Med. Chem. Lett. **2002**, 12.8, 1225-1227.
[36] T. F. Herpin, K. G. Van Kirk, J. M. Salvino, S. T. Yu and R. F. Labaudinière, J. Comb. Chem., **2000**, 2.5, 513-521.
[37] L. El Ghayati, Y. Ramli, A. Moussaif, J. Koubachi, M. L. Taha, E. M. Essassi and J. T. Mague. IUCrData., **2018**, 3, x180953.
[38] M.Salem, L.EL Ghayati, E.M.Essasi, Moroccan journal of Heterocyclic chemistry., **2018**, 17(2), 82-86.
[39] J.Sebhaoui, Y.El Bakri, Y.El Aoufir, El.H.Anoua, A.Guenbour, A.A.Nasser, E.M.Essasi, J. Mol. Struct., **2019**, 1182, 123-130.
[40] B. El Ibrahimi, A. Jmiai, L. Bazzi, and S. El Issami. Arab. J. Chem., **2020**, 13, 740-771.
[41] L.T. Popoola, Heliyon, **2019**, 5, e01143.
[42] I.B. Obot, K. Haruna, and T.A. Saleh, Arab. J. Sci. Eng. **2018**.
[43] P. Dohare, K.R. Ansari, M.A. Quraishi, and I.B. Obot, J. Ind. Eng. Chem., **2017**, 52, 197–210.
[44] C. Verma, L.O. Olasunkanmi, E.E. Ebenso, M.A. Results Phys., **2018**, 8, 657–70.
[45] P. M. Kanyonga, M. Y. A. Faouzi, A. Zellou, M. E. Essassi, and Y. Cherrah, Int. j. biol. chem. sci , **2009**, 3(4), 646–652, 2009.
[46] R. Dennington, T. Keith, J. Millam, GaussView, version 5, Semichem Inc.: Shawnee Mission, KS., **2009**.
[47] M. Frisch, G. Trucks, H.B. Schlegel, G.E. Scuseria, M.A. Robb, J.R. Cheeseman, G. Scalmani, V. Barone, B. Mennucci, G. Petersson, Gaussian 09, revision D. 01, Gaussian, Inc., Wallingford CT., **2009**.
[48] C Lee, W Yang, Physical review. B., **1988**, 37.2, 785.
[49] R. Jain, B. Ahuja, B. Sharma, Indian J. Pure Appl. Phys., **2004**, 42, 43-48.
[50] C. Lee, W. Yang, R. Parr, Phys. l rev. b., **1988**, 37, 785.
[51] M. Prasath, S. Muthu, R.A. Balaji, Spectrochimica Acta Part A: Molecular and Biomolecular Spectroscopy. **2013**, 113, 224-235.
[52] O. Trott, A.J. Olson, J. Comput. Chem ., **2010**, 31.2, 455-461.
[53] Y. Sert, A.A. El-Emam, O.A. Al-Deeb, A.A. Al-Turkistani, F. Ucun, Ç. Çırak, Molecular and Biomolecular Spectroscopy., **2014**, 126, 86-97.
[54] M. Turner, J. McKinnon, S. Wolff, D. Grimwood, P. Spackman, D. Jayatilaka, M.A. Spackman, CrystalExplorer17., **2017**.
[55] F.L. Hirshfeld, Theoretica chimica acta., **1977**, 44.2, 129-138.
[56] J.J. McKinnon, M.A. Spackman, A.S. MitchellActa Crystallographica Section B: Structural Science., **2004**, 60.6, 627-668.
[57] M.A. Spackman, P.G. Byrom, Chem. Phys. Lett., **1997**, 267(3-4), 215-220.
[58] M. Haghdadi, F.S. Kenary, H. Basra, Organic Chemistry, An Indian Journal., **2014**, 2014, 10.
[59] R. Ditchfield, Self-consistent perturbation theory of diamagnetism: I. Molecular Physics., **1974**, 27.4, 789-807.
[60] K. Wolinski, J.F. Hinton, P. Pulay, J. Am. Chem. Soc., **1990**, 112(23), 8251-8260
[61] https://www.rcsb.org/.
[62] D.-Q. Wei, J.-F. Wang, C. Chen, Y. Li, K.-C. Chou, Protein Pept. Lett., 2008, 15.1, 27-32.
[63] https://www.3dsbiovia.com/.

[64] J.O. Bockris, and A.K.N. Reddy, Modern Electrochemistry. 2nd ed edn. Vol. 2B New York/Boston, USA: Kluwer Academic/Plenum Publishers, **2000**.
[65] B. El Ibrahimi, A. Jmiai, K. El Mouaden, R. Oukhrib, A. Soumoue, S. El Issami, and L. Bazzi, J. King Saud Univ. Sci., **2020,** 32, 163-71.
[66] B. El Ibrahimi, A. Jmiai, K. El Mouaden, A. Baddouh, S. El Issami, L. Bazzi, and M. Hilali, J. Mol. Struct., **2019**, 1196, 105-18.
[67] V. Fabian, Simulated Annealing Simulated, Comput. Math. Appl., **1997**, 33, 81-94.
[68] H. Bourzi, R. Oukhrib, B.E. Ibrahimi, H.A. Oualid, Y. Abdellaoui, B. Balkard, S.E. Issami, M. Hilali, L. Bazzi, and C. Len, Sustainability, **2020**, 12, 3304.
[69] R. Oukhrib, B. El Ibrahimi, H. Abou Oualid, Y. Abdellaoui, S. El Issami, L. Bazzi, M. Hilali, and H. Bourzi, J. Mol. Liq., **2020**. doi 10.1016/j.molliq.2020.113479
[70] A. Jmiai, B. El Ibrahimi, A. Tara, S. El Issami, O. Jbara, and L. Bazzi, J. Mol. Struct., **2018**, 1157, 408-17.
[71] K. Abderrahim, I. Selatnia, A. Sid, and P. Mosset, Chem. Phys. Lett., **2018**, 707, 117–28.
[72] M.E. Mashuga, L.O. Olasunkanmi, and E.E. Ebenso, J. Mol. Struct., **2017**, 1136, 127-39.
[73] Y.N. Mabkhot, F. Alatibi, N.N.E. El-Sayed, N.A. Kheder, S.S. Al-Showiman, Molecules., **2016**, 21, 1036.
[74] K. Hoffmann, J. Wiśniewska, A. Wojtczak, J. Sitkowski, A. Denslow, J. Wietrzyk, M. Jakubowski, I. Łakomska, J. Inorg. Biochem., **2017**, 172, 34-45.
[75] S.M. Finegold, W.J. Martin, Diagnostic Microbiology: Bailey and Scott's, Sixth ed., CV Mosby. **1982**.
[76] D. Alderman, P. Smith, Aquaculture., **2001**, 196(3-4), 211-243.
[77] L. El Ghayati, N. H. Ahabchane, M. L. Doumbia, N. K. Sebbar, E. M. Essassi and J. T. Mague., IUCrData., **2017**, 2.1, x161998.